Journal of Thermal Analysis and Calorimetry (2021) 143:767–779
https://doi.org/10.1007/s10973-019-09146-z

Effects of nanoparticle shape and size on the thermohydraulic performance of plate evaporator using hybrid nanofluids

Atul Bhattad[1] · **Jahar Sarkar**[1]

Received: 14 August 2019 / Accepted: 1 December 2019 / Published online: 9 December 2019

Abstract

Brines (ethylene glycol, calcium chloride, propylene glycol and potassium acetate)-based hybrid (combinations of alumina, copper oxide, silica and titania with copper nanoparticles) nanofluids have been used as a secondary refrigerant to improve the heat transfer characteristics of the plate evaporator for milk chilling. Effect of nanoparticle combination, shape and size on heat transfer area, pump work, the ratio of heat transfer coefficient to pressure drop, coefficient of performance, performance index, thermal performance factor and exergetic efficiency has been examined theoretically. Copper oxide–copper hybrid nanofluid gives superior performance, while silica–copper hybrid nanofluid performs well in terms of exergetic efficiency. The maximum decrease in effective heat transfer area (5.9%) is found for propylene glycol brine-based copper oxide hybrid nanofluid. Percentage change in heat transfer area and performance index reduces with an increase in the particle size and is maximum for alumina–copper hybrid nanofluid. However, thermal performance factor increases with particle size. Brick-shaped particles show maximum changes in heat transfer area and performance index, while platelet-shaped particles show worse performance. The study reveals that the nanoparticle shape has a strong influence on the plate heat exchanger performance due to a significant deviation in surface area-to-volume ratio.

Keywords Hybrid nanofluid · Secondary refrigerant · Plate evaporator · Nanoparticle size · Nanoparticle shape · Performance parameter

List of symbols

A	Heat transfer area (m^2)
b	Mean channel spacing (mm)
c_p	Specific heat (J kg^{-1} K^{-1})
D	Diameter (mm)
D_h	Hydraulic diameter (m)
E	Exergy rate (W)
f	Friction factor (dimensionless)
G	Mass velocity (kg s^{-1} m^{-2})
h	Specific enthalpy (J kg^{-1})
J	Comparison factor (m s^{-1} K^{-1})
k	Thermal conductivity (W m^{-1} K^{-1})
L	Length (m)
$\dot{m}$	Mass flow rate (kg s^{-1})
M	Molecular weight
n	Shape function (dimensionless)
N	Avogadro number ($mole^{-1}$)
N_p	Number of passes (dimensionless)
N_t	Number of plates (dimensionless)
Nu	Nusselt number (dimensionless)
p	Pressure (Pa)
Q	Heat transfer rate (W)
r	Radius (nm)
s	Specific entropy (J K^{-1})
T	Temperature (K)
t	Plate thickness (mm)
U	Overall heat transfer coefficient (W K^{-1} m^{-2})
W	Work transfer rate (W)

Abbreviation

Al_2O_3	Alumina
$CaCl_2$	Calcium chloride
CuO	Copper oxide
COP	Coefficient of performance
EES	Engineering equation solver
EG	Ethylene glycol
HyNf	Hybrid nanofluid
KAC	Potassium acetate
LMTD	Log mean temperature difference
MWCNT	Multiwalled carbon nanotube

✉ Jahar Sarkar
jsarkar.mec@itbhu.ac.in

[1] Department of Mechanical Engineering, Indian Institute of Technology (B.H.U.), Varanasi, UP 221005, India

PHE	Plate heat exchanger
PG	Propylene glycol
PI	Performance index
TiO_2	Titania
TPF	Thermal performance factor
v%	Volume percentage

Greek symbols

α	Heat transfer coefficient (W K^{-1} m^{-2})
β	Chevron angle (°)
ρ	Density (kg m^{-3})
η	Efficiency (dimensionless)
Ω	Coefficient (dimensionless)
Φ	Volume fraction (dimensionless)
μ	Dynamic viscosity (Pa s)

Subscripts

II	Second
a	First particle
b	Second particle
bf	Basefluid
ch	Channel
comp	Compressor
e	Ambient
eva	Evaporator
i	Inlet
nf	Hybrid nanofluid
o	Outlet
p	Port
r	Refrigerant

Introduction

Issues such as depletion of energy resources and environmental temperature rise lead to the direction of the study on the improvement in thermal systems and heat transfer fluids with enhanced thermo-physical and transport characteristics. To reduce the primary refrigerant leakage-related environmental problem, secondary refrigerants such as various glycols and salt solutions have been implemented for the secondary loop refrigeration [1]. Water-based solution (brine) of ethylene glycol (EG), propylene glycol (PG), calcium chloride ($CaCl_2$) and potassium acetate (KAC) is widely used as a secondary refrigerant [2]. Nanofluids have been emerging as an innovative fluid because of excellent heat transfer characteristics and heat exchanger size reduction, which make them suitable for various applications [3–5]. Recently, hybrid nanofluids (HyNfs) are also getting importance due to their enhanced transport properties and heat transfer behavior due to hybridization [6, 7]. The thermal conductivity can be considerably improved by using mono as well as hybrid nanofluids [8–10], which leads to their application in various thermal and chemical systems [11–13]. The improvement in heat transfer performance using hybrid nanofluids can be adjusted by altering the nanoparticle mixture ratio [14, 15]. Either the size of the thermal system or the pumping power of the existing system can be reduced by using hybrid nanofluids [16]. Plate heat exchangers are broadly operated in many food processing applications, and the performance of plate heat exchanger can be significantly improved by using nanofluids with optimum nanoparticle concentration [17]. Huang et al. [18] observed the enhancements in pressure drop and heat transfer coefficient using MWCNT-Al_2O_3/water hybrid nanofluid in the plate heat exchanger. Kumar et al. [19] performed the energetic and exergetic analyses on the plate heat exchanger with various plate spacings using Cu–Al_2O_3/water hybrid nanofluids and showed the best performance for 5-mm plate spacing. Bhattad et al. [20] observed that the performance of refrigeration unit is enhanced using HyNf as a secondary refrigerant in plate evaporator. Kumar et al. [21] performed an exergetic analysis on the plate heat exchanger with different MWCNT–water hybrid nanofluids and observed that CeO_2–MWCNT/water hybrid nanofluid could be a suitable coolant as it yields maximum reduction of exergy loss by 24.75%. Through theoretical studies on plate heat exchanger, Bhattad et al. [22, 23] concluded that brine-based hybrid nanofluid yields better energy–exergy performances as a secondary refrigerant or coolant. These facts have motivated to use brine-based hybrid nanofluids as a secondary refrigerant.

The investigation of different nanoparticle shapes and sizes is also crucial as they affect various properties of the nanofluids. Different authors studied the influence of particle shape and size on rheological behavior and properties such as density, specific heat capacity, dynamic viscosity, thermal conductivity [24–31] and the heat transfer performance of the heat exchangers [32–35]. Timofeeva et al. [25] observed that elongated nanoparticles such as cylindrical and platelet-shaped result in increased viscosity. Xie et al. [36] saw a drop in the thermal conductivity of nanofluids with an increase in particle size. Kim et al. [37] found that the thermal conductivity of nanofluids rises linearly with a decrease in the particle radius. The particle size becomes significant in the case of higher particle concentrations [38]. Mintsa et al. [39] measured the thermal conductivity of Al_2O_3 and CuO nanofluids and revealed that the effective thermal conductivity increases with a rise in particle addition and with a reduction in particle size. Monfared et al. [40] conducted a second law analysis of a double-tube heat exchanger with different nanoparticle shapes and observed the best performance with a spherical shape. Related previous works are summarized in Table 1, and as shown, only shape effect has been studied for heat exchangers; no work on nanoparticle size effect is available. Also, to the best of the authors' knowledge, the impact of nanoparticle size and

Table 1 Previous studies on heat exchanger with different shape/size nanoparticles

References	Device	Nanofluid, investigation	Findings
Elias et al. [32]	Shell and tube heat exchanger	Alumina/EG brine, nanoparticle shape effect	Cylindrical shape yields best performance
Mahian et al. [33]	Minichannel solar collector	Alumina/EG brine, nanoparticle shape effect	Entropy generation is minimum for the brick shape
Arani et al. [34]	Sinusoidal–wavy minichannel	Alumina/EG brine, nanoparticle shape effect	Highest performance evaluation criterion for the spherical shape
Hajabdollahi and Hajabdollahi [35]	Shell and tube heat exchanger	Alumina/water, nanoparticle shape effect	Thermo-economic parameters are improved higher for brick shape
Monfared et al. [40]	Double-pipe heat exchanger	Alumina/EG brine, nanoparticle shape effect	Lowest frictional entropy generation for the spherical shape

shape has not been studied yet for nanofluids in the plate heat exchanger.

Hence in this paper, a theoretical analysis has been performed to explore the effects of nanoparticle shape and size on the energoexergy characteristics of the corrugated, counterflow plate-type heat exchanger as an evaporator with different brine-based hybrid nanofluids as the secondary refrigerant for milk chiller application. Studied hybrid nanofluids comprise different nanoparticles (the combination of a metal particle with ceramic particles) such as CuO, SiO_2, Al_2O_3 and TiO_2 with Cu nanoparticles, mixed in equal particle volume in the base fluid (total concentration of 0.8 v%). The different base fluids comprise different brine solutions in distinct percentages, maintaining consistent freezing temperature. The evaporator capacity has been taken as 50 kW. Influence of varying brine solution and nanoparticle combination on the heat transfer area, pumping power, comparison factor, coefficient of performance, performance index, second law efficiency and thermal performance factor has been analyzed. The consequence of particle size (average diameter varying from 10 to 50 nm) and particle shape (spherical, cylindrical, brick and platelet) has been investigated on the heat exchanger area, performance index and thermal performance factor.

Methodology

Modeling procedure and simulation

In the present theoretical investigation, a corrugated, counterflow-type plate heat exchanger (PHE) exchanging heat between the secondary refrigerant (brine-based hybrid nanofluid) and primary refrigerant (ammonia) has been considered as an evaporator. The study is concerned with milk chilling application. A block diagram of the refrigeration system (with the secondary loop) is shown in Fig. 1. Evaporator, condenser, nanofluid inlet and outlet temperatures have been chosen as 0 °C, 40 °C, 20 °C and 5 °C, respectively, for milk chilling unit. Properties of ammonia

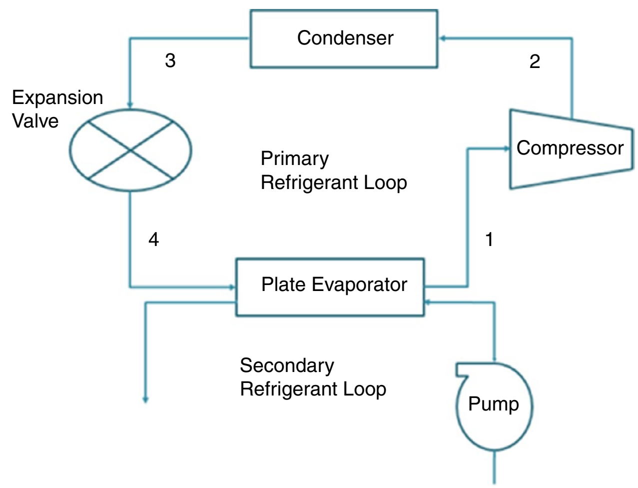

Fig. 1 Block diagram of secondary loop refrigeration system

and base fluids have been acquired from EES Library [41], whereas properties of nanoparticles have been taken from the literature and are shown in Table 2. The hybrid nanofluid sample was assumed to be stable and homogeneous for a longer period. Different particle sizes (10–50 nm) and different particle shapes (brick, sphere, cylinder and platelet) have been taken to show their effects.

Modeling has been performed based on heat capacity and heat transfer rate equations. For this, the overall heat transfer coefficient has been determined by,

$$U = \frac{1}{\frac{1}{\alpha_r} + \frac{1}{\alpha_{nf}} + \frac{t}{k_w}} \tag{1}$$

where t is the plate thickness, α_r is the heat transfer coefficient of refrigerant, α_{nf} is the heat transfer coefficient of hybrid nanofluid, U is the overall heat transfer coefficient and k_w is the thermal conductivity of plate.

The formulation for the calculation of mass flow rate of primary and secondary refrigerants, heat transfer coefficient and pressure drop is taken from Bhattad et al. [22,

Table 2 Thermo-physical properties of different nanoparticles and base fluids (20 °C)

Nanoparticles/base fluids	Thermal conductivity/W m^{-1} K^{-1}	Specific heat/J kg^{-1} K^{-1}	Density/kg m^{-3}	Viscosity/Pa s
Al_2O_3	36.6	752	3970	
CuO	17.2	548	6315	
TiO_2	8.5	703	4160	
SiO_2	1.38	738	2202	
Cu	401.7	383	8936	
EG/water (15%)	0.53	4004	1018	0.001456
PG/water (17%)	0.51	4050	1012	0.001859
$CaCl_2$/water (10%)	0.59	3608	1083	0.00128
KAC/water (12%)	0.56	3751	1059	0.00135

23]. The heat exchanger area has been estimated from Eq. (2).

$$Q = \frac{UA((T_{\text{nfi}} - T_{\text{eva}}) - (T_{\text{nfo}} - T_{\text{eva}}))}{\ln \frac{(T_{\text{nfi}} - T_{\text{eva}})}{(T_{\text{nfo}} - T_{\text{eva}})}} \tag{2}$$

The combined effect of heat transfer coefficient and pressure drop due to the application of nanoparticles has been studied through the comparison factor, J, which is a ratio of heat transfer coefficient to the pressure drop.

$$J = \alpha / \Delta p \tag{3}$$

Pump work and compressor work are given by,

$$W_{\text{pump}} = \dot{m}_{\text{nf}} \Delta p_{\text{nf}} / \rho_{\text{nf}} \eta_{\text{pump}} \text{ and } W_{\text{comp}} = \dot{m}_{\text{r}}(h_2 - h_1) \tag{4}$$

The coefficient of performance (COP) is defined as the ratio of heat transfer rate and power required by pump and compressor, and is given by

$$\text{COP} = Q / (W_{\text{comp}} + W_{\text{pump}}) \tag{5}$$

The performance index, a dimensionless number, is a ratio of heat transfer rate to pump work, which is given by,

$$\text{PI} = Q / W_{\text{pump}} \tag{6}$$

The relevance of heat transfer and pressure drop characteristics is shown using thermal performance factor (TPF) [42],

$$\text{TPF} = \left(\frac{\text{Nu}_{\text{nf}}}{\text{Nu}_{\text{bf}}} \right) \Big/ \left(\frac{f_{\text{nf}}}{f_{\text{bf}}} \right)^{\frac{1}{3}} \tag{7}$$

Nusselt number and friction factor for hybrid nanofluid and base fluid are calculated using the correlations given by Huang et al. [43] and Kakac and Liu [44]. The formulations for exergetic modeling and exegetic efficiency calculation of brine-based hybrid nanofluids are taken from Bhattad et al. [22, 23].

The density and specific heat capacity of hybrid nanofluids containing all types of nanoparticles have been calculated by, respectively,

$$\rho_{\text{nf}} = \Phi_{\text{b}} \rho_{\text{b}} + \Phi_{\text{a}} \rho_{\text{a}} + (1 - \Phi) \rho_{\text{bf}} \tag{8}$$

$$\rho_{\text{nf}} c_{\text{pnf}} = \Phi_{\text{b}} \rho_{\text{b}} c_{\text{p,b}} + \Phi_{\text{a}} \rho_{\text{a}} c_{\text{p,a}} + (1 - \Phi) \rho_{\text{bf}} c_{\text{p,bf}} \tag{9}$$

where $\Phi = \Phi_a + \Phi_b$

The size/shape of the particle significantly affects the transport properties of hybrid nanofluid. To show the consequence of particle size (mean radius) on different parameters, the following correlations were used for estimation of thermal conductivity [45] and dynamic viscosity [46, 47] of hybrid nanofluids.

$$k_{\text{nf}} = \left[k_{\text{bf}} + \frac{r_{\text{bf}} \Phi_{\text{a}} k_{\text{a}}}{r_{\text{a}}(1 - \Phi)} + \frac{r_{\text{bf}} \Phi_{\text{b}} k_{\text{b}}}{r_{\text{b}}(1 - \Phi)} \right] \tag{10}$$

$$\mu_{\text{nf}} = \left(\mu_{\text{nfa}} \Phi_{\text{a}} + \mu_{\text{nfb}} \Phi_{\text{b}} \right) / \Phi \tag{11}$$

$$\frac{\mu_{\text{nfa}}}{\mu_{\text{bf}}} = \frac{1}{1 - 34.87 \left(\frac{r_{\text{bf}}}{r_{\text{a}}} \right)^{0.3} \Phi^{1.03}} \tag{12}$$

$$\frac{\mu_{\text{nfb}}}{\mu_{\text{bf}}} = \frac{1}{1 - 34.87 \left(\frac{r_{\text{bf}}}{r_{\text{b}}} \right)^{0.3} \Phi^{1.03}} \tag{13}$$

$$r_{\text{bf}} = \frac{\left[\frac{6M}{\pi N \rho_{\text{bf}}} \right]^{\frac{1}{3}}}{2} \tag{14}$$

where r = radius in nm, M = molecular weight and N = Avogadro number.

Different particle shapes such as sphere, cylinder, brick and platelet have been taken for the investigation purpose. To show the effect of particle shape on various parameters,

Table 3 Value of shape factor (n) for different shapes [48]

Particle shape	Brick	Cylinder	Platelet	Sphere
Shape factor (n)	3.7	4.8	5.7	3

Table 4 Value of coefficients (Ω_1 and Ω_2) for different shapes [49]

Coefficient	Brick	Cylinder	Platelet
Ω_1	1.9	13.5	37.1
Ω_2	471.4	904.4	612.6

the following models were used for thermal conductivity [48] and dynamic viscosity [47, 49].

$$\frac{k_{\mathrm{nf}}}{k_{\mathrm{bf}}} = \left(\frac{k_{\mathrm{a}} + (n_{\mathrm{a}} - 1)k_{\mathrm{bf}} - (n_{\mathrm{a}} - 1)(k_{\mathrm{bf}} - k_{\mathrm{a}})\Phi_{\mathrm{a}}}{k_{\mathrm{a}} + (n_{\mathrm{a}} - 1)k_{\mathrm{bf}} + (k_{\mathrm{bf}} - k_{\mathrm{a}})\Phi_{\mathrm{a}}}\right) \left(\frac{k_{\mathrm{b}} + (n_{\mathrm{b}} - 1)k_{\mathrm{nf}} - (n_{\mathrm{b}} - 1)(k_{\mathrm{nf}} - k_{\mathrm{b}})\Phi_{\mathrm{b}}}{k_{\mathrm{b}} + (n_{\mathrm{b}} - 1)k_{\mathrm{nf}} + (k_{\mathrm{nf}} - k_{\mathrm{b}})\Phi_{\mathrm{b}}}\right) \tag{15}$$

$$\frac{\mu_{\mathrm{nf}}}{\mu_{\mathrm{bf}}} = \frac{\Phi_{\mathrm{a}}}{\Phi}\left(1 + \Omega_{1,\mathrm{a}}\Phi + \Omega_{2,\mathrm{a}}\Phi^2\right) + \frac{\Phi_b}{\Phi}\left(1 + \Omega_{1,\mathrm{b}}\Phi + \Omega_{2,\mathrm{b}}\Phi^2\right) \tag{16}$$

where n_{a} and n_{b} are shape factors whose values are given in Table 3 [48].

Ω_1 and Ω_2 are coefficients whose values are provided in Table 4 [49].

It has been assumed that both the particles, in a particular hybrid nanofluid, are of the same size and the same shape. Engineering equation solver [41] has been used for simulation purposes because of its easiness in use and inbuilt library function.

Model validation

The simulation model has been authenticated with own experimental data. The layout and picture of the experimental facility are shown in Figs. 2 and 3, respectively, which contains cold and hot fluid circuits. The test section is commercial PHE made of stainless steel having 5 hot channels, 4 cold channels, a mean channel spacing of 2.8 mm, an active heat transfer area of 0.3 m^2 and a plate thickness of 0.5 mm. Isothermal baths have been used in both circuits to maintain desired inlet temperatures. Volume flow rates, temperatures and pressure drops in both loops have been measured by float type flowmeter, thermocouples and U-tube manometers, respectively. After setting inlet temperatures and flow rates of both hot and cold fluids, all the measuring parameters have been recorded at the steady-state condition. For the validation, the cold and hot streams inlet temperature has been selected as 20 °C and 50 °C, respectively, with the flow rate of both streams as 3 lpm. Water has been taken as fluid on both loops. The heat exchanger area obtained from the theoretical investigation (0.275 m^2) is validated with that in the experimental study (0.3 m^2) with a deviation of around

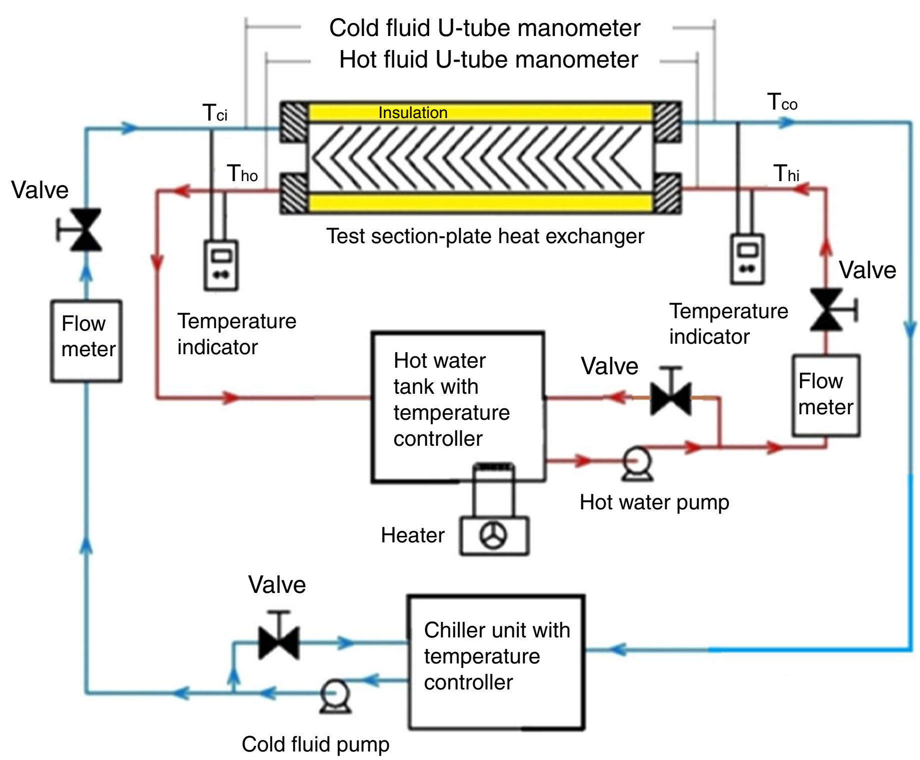

Fig. 2 Layout of plate heat exchanger experimental setup [15]

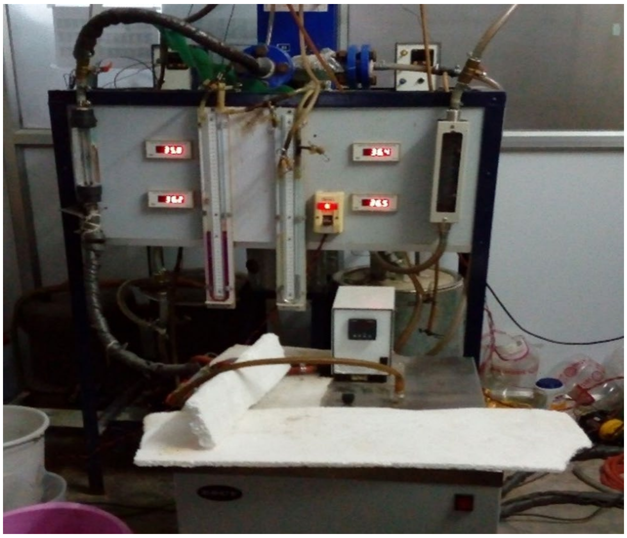

Fig. 3 Photograph of plate heat exchanger experimental setup [15]

8.33%, which is justified due to the assumptions made. For the results of the present simulation, the same dimensions of the experimental setup have been taken for plate evaporator.

Results and discussion

Figure 4 depicts the comparison of the required heat transfer area in the milk chilling unit for various base fluids as well as the corresponding hybrid nanofluids. Among the base fluids, the heat exchanger plate area required is observed minimum for $CaCl_2$ brine followed by KAC, EG and PG brines [22]. However, the heat transfer area decreases while using hybrid nanofluids due to augmentation in the overall heat transfer coefficient. The same trend has been depicted for the hybrid nanofluid, i.e., $CaCl_2$ brine HyNf requires the least heat transfer plate area followed by KAC, EG and PG brine. Moreover, PG brine HyNf shows a maximum (5.91%) and $CaCl_2$ brine HyNf shows minimum (4.47%) reduction in the heat transfer area. Likewise, CuO–Cu HyNf combination shows a maximum decrease in active plate area, while other combinations show almost the same reduction.

Figure 5 depicts the variation of the comparison factor (ratio of heat transfer coefficient and pressure drop) for various base fluids and the corresponding HyNfs. Among the base fluids, $CaCl_2$ brine yields the maximum comparison factor and PG brine yields the minimum comparison factor. Moreover, silica oxide–PG hybrid nanofluids show the highest improvement (49.3%) and copper oxide–PG hybrid nanofluids show the least improvement (48.6%) as compared to corresponding base fluids. This is due to the combined effect of an increase in heat transfer coefficient and a decrease in pressure drop while adding nanoparticles in the base fluids. The heat transfer coefficient rises due to increased mass velocity and Reynolds number. This dissimilarity results from the collective thermo-physical possessions of both the particles. Also, the pressure drop decreases due to the dual effect of a change in density and viscosity at low temperatures. Pressure drop also decreases due to the decrease in the flow length of the heat exchanger.

Figure 6 indicates the variation of pump work required for different fluids. Between the base fluids, PG brine shows the maximum reduction in pumping power required, trailed by EG, KAC and $CaCl_2$ brine [22, 23]. Higher pump work necessitates higher energy dissipation. The pump work requirement has been observed less for the hybrid nanofluid as compared to the relevant base fluid. Hence, hybrid nanofluids reduce the pump work for low temperatures. PG brine offers a maximum reduction in pump work (3.69%) followed by EG, KAC and $CaCl_2$ brine. Reduction in pump work is maximum for silica hybrid nanofluid and minimum for CuO hybrid nanofluid. An enhancement in COP has been

Fig. 4 Comparison of heat transfer area

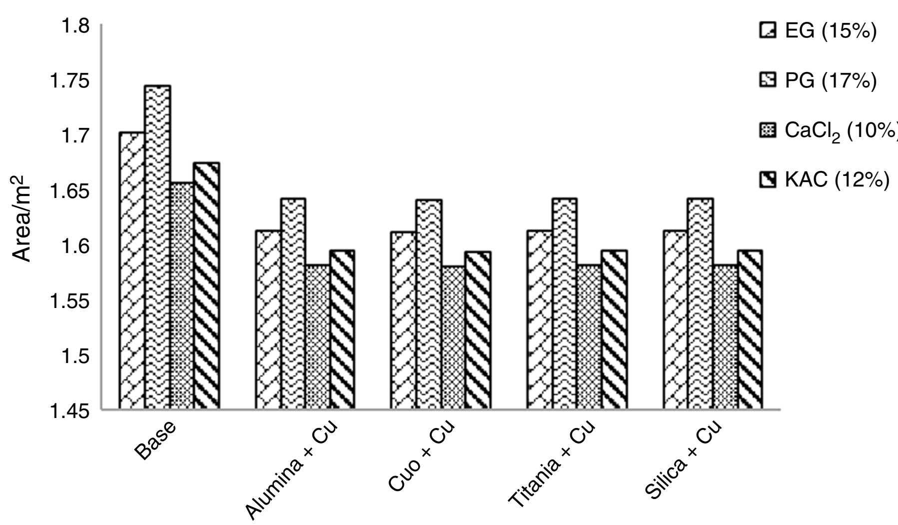

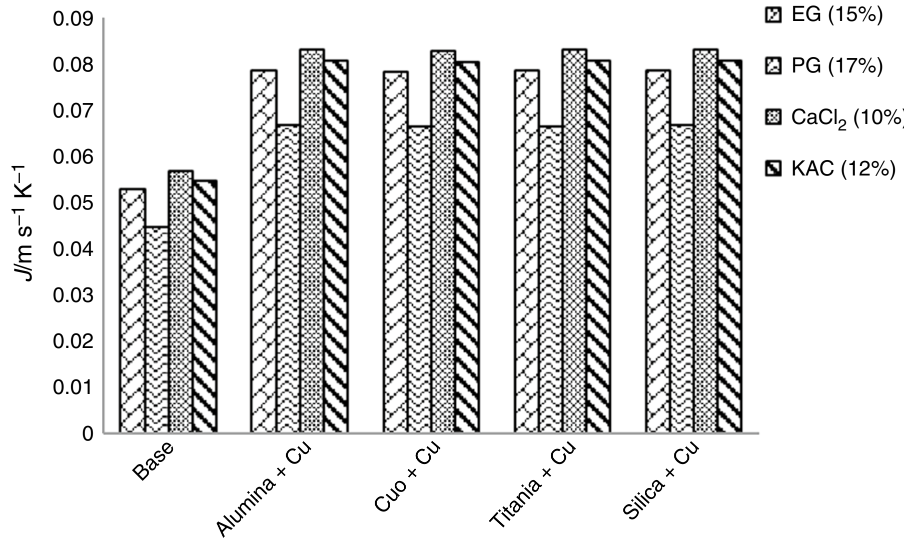

Fig. 5 Comparison of comparison factor

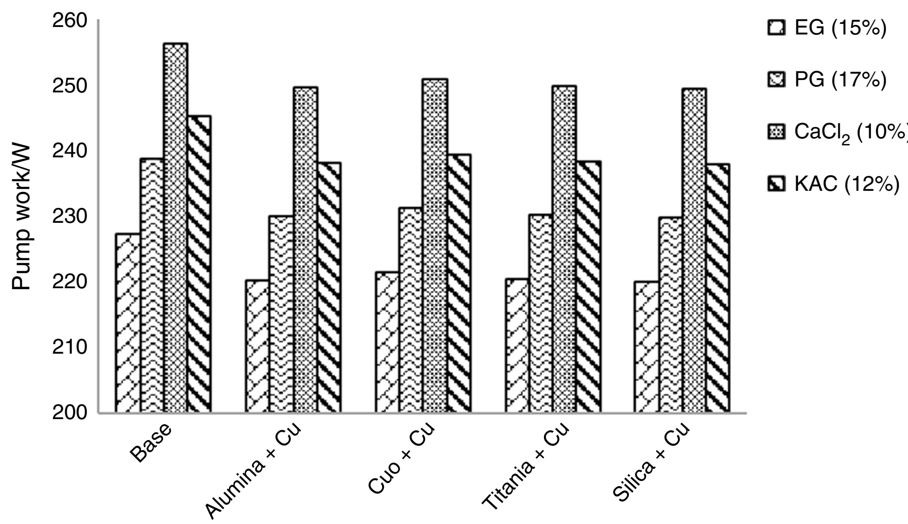

Fig. 6 Comparison of pump work

recognized while using hybrid nanofluids as shown in Fig. 7. The coefficient of performance was found the least for the $CaCl_2$ and highest for ethylene glycol. But percentage-wise, it is minimum for EG hybrid nanofluids and maximum for KAC hybrid nanofluids. Fluid with the highest pumping power gives the least performance index (Eq. 6) and exergetic efficiency. The variations of exergetic efficiency and performance index are shown in Figs. 8 and 9. The performance index is inversely proportional to the pumping power. The values of performance index and exergetic efficiency have been found high for EG brine and low for $CaCl_2$ brine solutions. While SiO_2–Cu–PG HyNf shows maximum improvement in performance index (3.96%) and exergetic efficiency (0.78%), CuO–Cu–$CaCl_2$ HyNf shows minimum improvement.

To show the comparative effect of pressure drop and heat transfer rate, a new parameter has been introduced, thermal performance factor (TPF) [42], which depends on the ratio of Nusselt number of nanofluid and base fluid, and the ratio of friction factor of nanofluid and base fluid. Figure 10 illustrates the thermal performance factor for the different brine-based hybrid nanofluids. Among the studied hybrid nanofluids, PG-based hybrid nanofluids give the highest and $CaCl_2$-based hybrid nanofluids provide the lowest value for thermal performance factor. Among PG-based hybrid nanofluids, CuO–copper hybrid nanofluids give the highest and silica–copper hybrid nanofluids give the lowest thermal performance factor. This is because the ratio of Nusselt number is more and that of friction factor is less for CuO–copper hybrid nanofluids followed by titania, alumina and silica hybrid nanofluids. As it has been found that in most of the cases PG-based hybrid nanofluid shows better performance, it has been chosen for further investigation. Figure 11 illustrates the effect of particle size (diameter) on the thermal

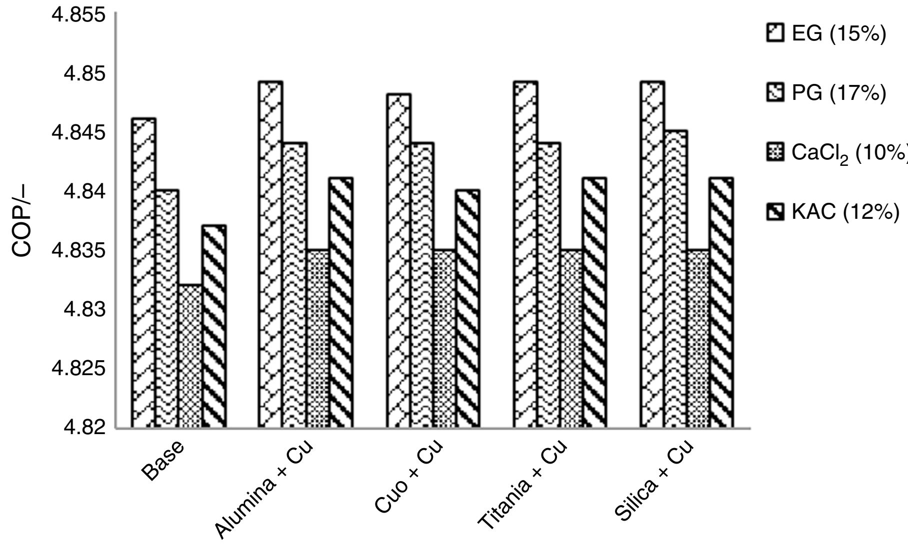

Fig. 7 Comparison of coefficient of performance

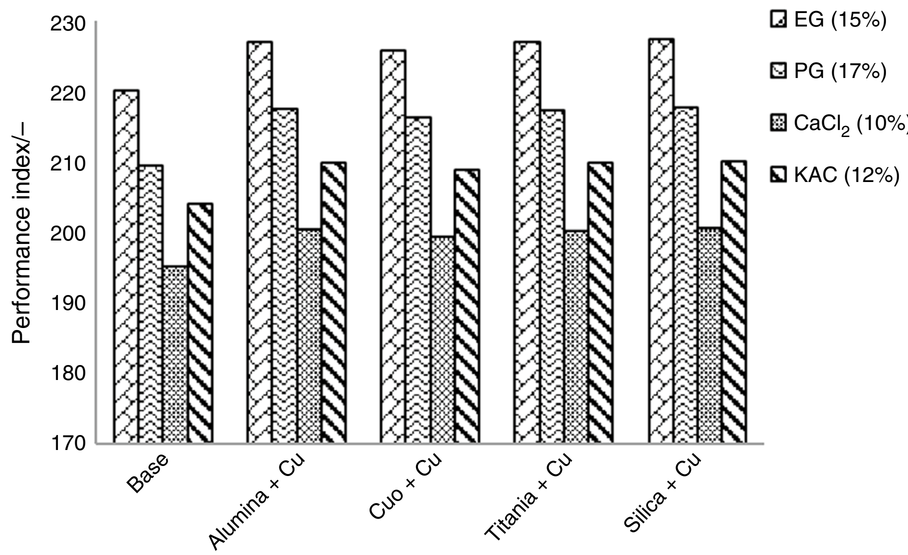

Fig. 8 Comparison of performance index

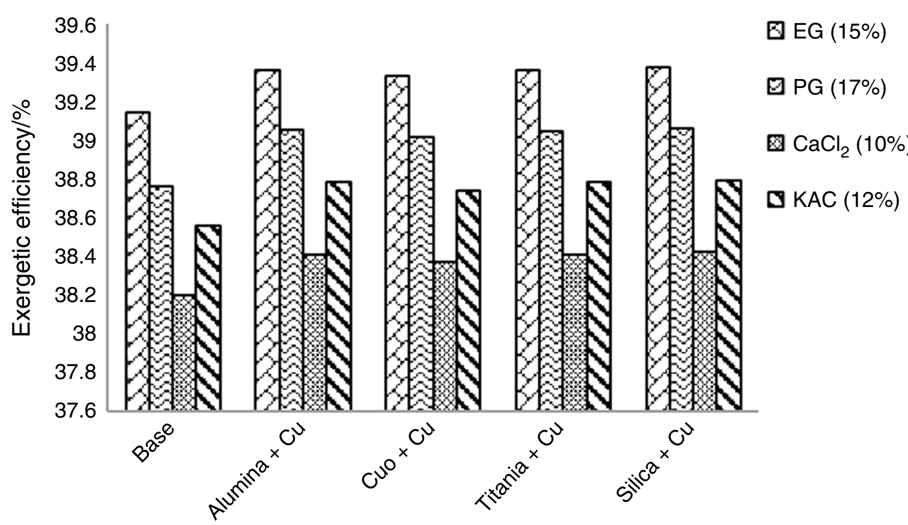

Fig. 9 Comparison of exergetic efficiency

Fig. 10 Comparison of thermal performance factor

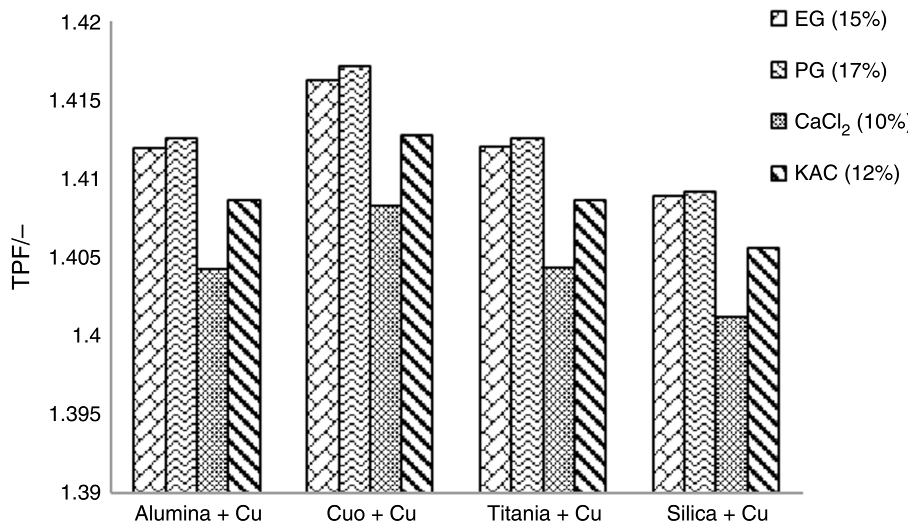

performance factor for the PG-based hybrid nanofluids. It was observed that as the particle size increases, the thermal performance factor rises and becomes maximum for the silica–copper combination and minimum for the alumina–copper combination. Similarly, Figs. 12 and 13 depict the dependency of particle size on the change in the area and the performance index of the heat exchanger, respectively. As the particle diameter increases, the percentage reduction in the area and percentage enhancement in the performance index decrease because with an increase in the size of the particle, its viscosity increases, which enhances the pressure drop and pump work, and hence degrades the performance index. Among the hybrid combinations, the percentage reduction in the area has been found the maximum for the alumina–copper hybrid nanofluid (12.8%) and minimum for the silica–copper combination (12.56%). Alumina–copper hybrid nanofluid shows the maximum change (13.75%) and CuO–copper shows the minimum change (12.94%) in the performance index.

Particle shape also plays a vital role in the performance characteristics of the heat exchanger. Their effect can be seen in the thermo-physical properties of the hybrid nanofluids. Different shapes such as brick, sphere, cylinder and platelet have been considered. Among these shapes, brick-shaped particles give the best performance followed by spherical and cylindrical shapes; and platelet-shaped particles give the least performance. Figure 14 shows the effect of particle shape on the thermal performance factor for the PG-based hybrid nanofluids. Among the hybrid combinations, alumina–copper gives the least and CuO–copper hybrid nanofluid gives the highest value of thermal performance factor. Figures 15 and 16 show the effect of particle shape on the change in the area and the performance index of the heat exchanger, respectively.

Fig. 11 Effect of particle size on thermal performance factor

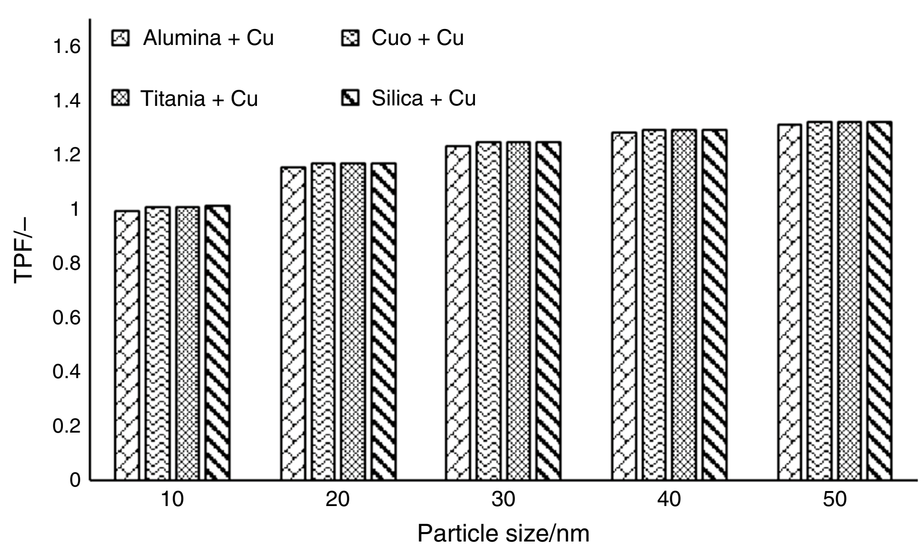

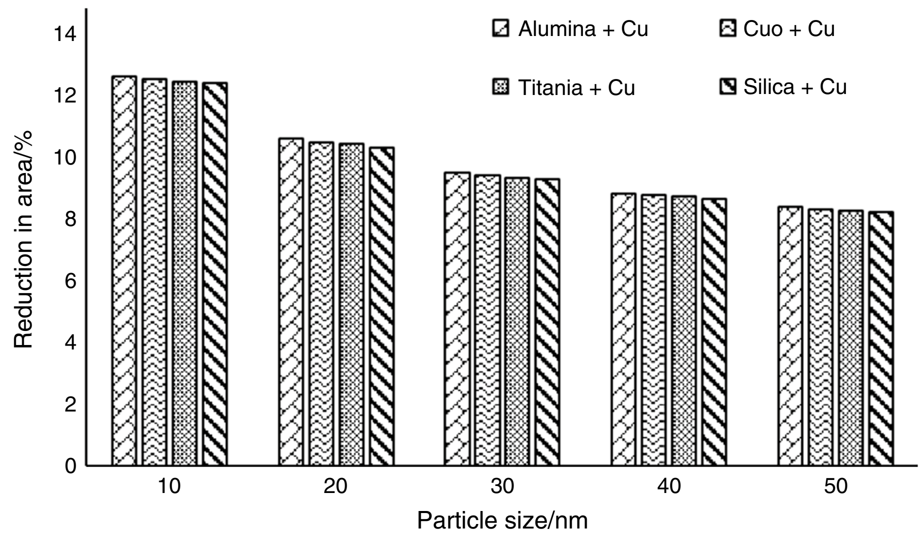

Fig. 12 Effect of particle size on percentage reduction in area

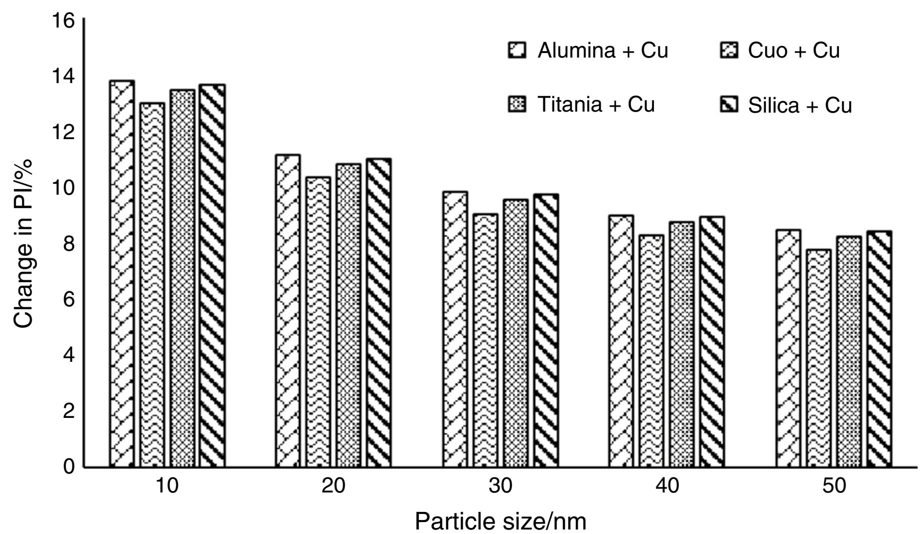

Fig. 13 Effect of particle size on percentage change in performance index

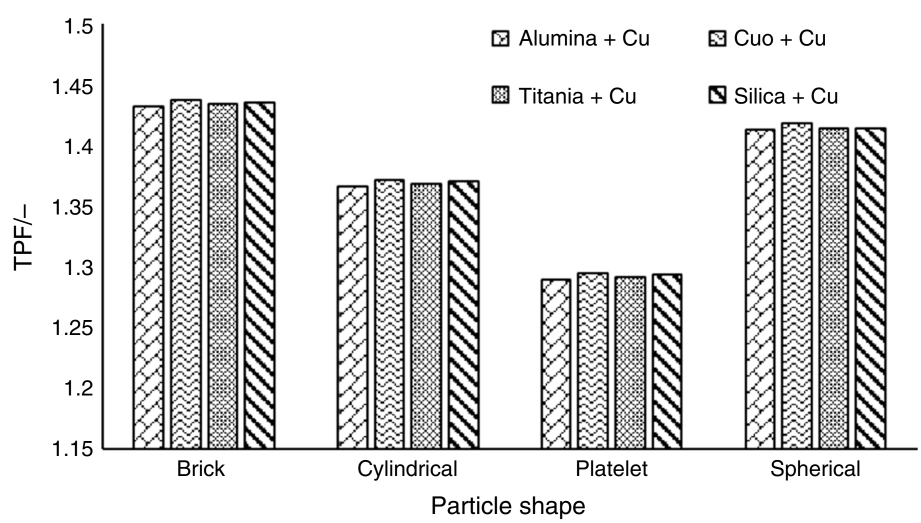

Fig. 14 Effect of particle shape on thermal performance factor

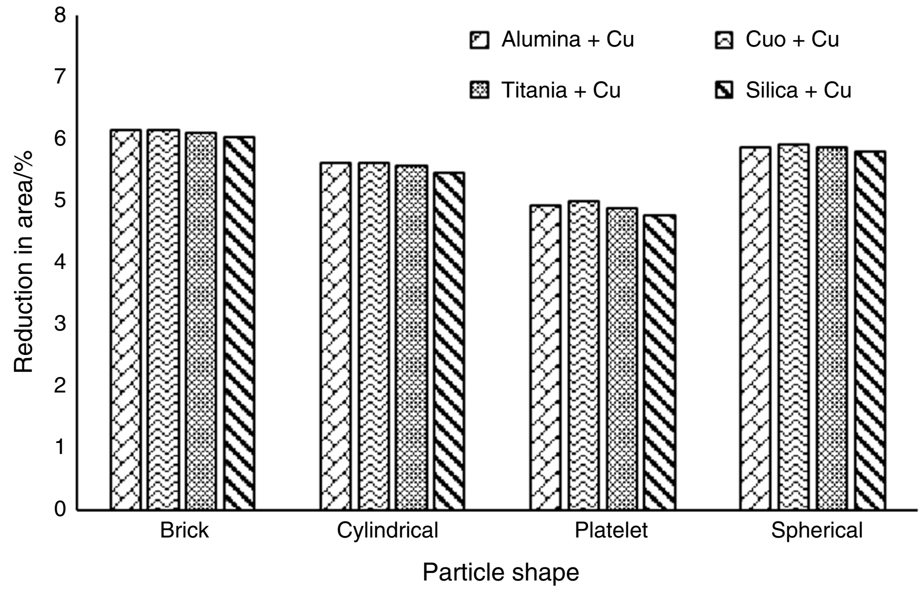

Fig. 15 Effect of particle shape on percentage reduction in area

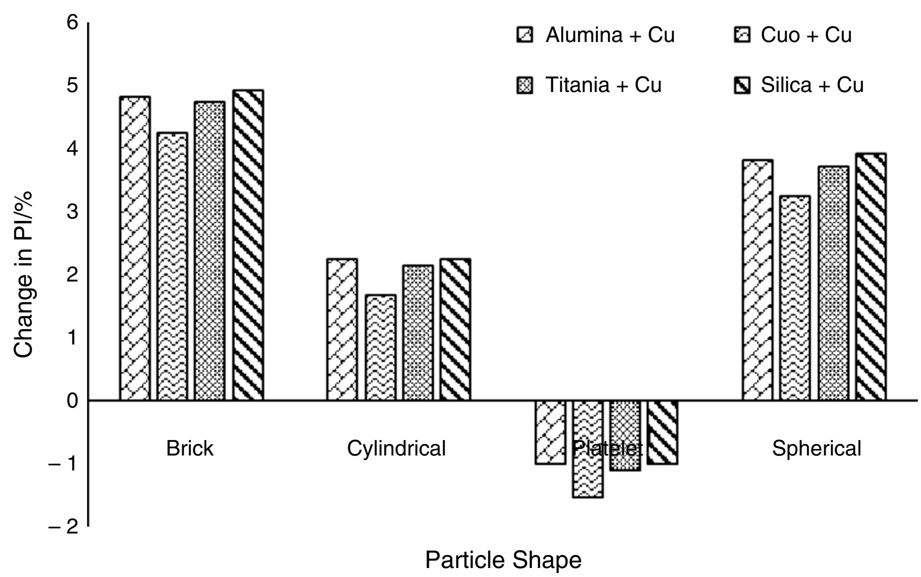

Fig. 16 Effect of particle shape on percentage change in performance index

Maximum area reduction was obtained for CuO–copper (6.14% brick shape) and minimum for silica–copper (4.76% platelet shape) hybrid nanofluids. Most of the shapes show an increment in the performance index except platelet shape. Platelet-shaped particles show a decrement in the performance index because the viscosity of hybrid nanofluid with this shaped nanoparticle is more in comparison with hybrid nanofluid with other shape nanoparticles. Maximum enhancement was observed for silica–copper, and maximum decrement was observed for copper oxide–copper hybrid nanofluids. So, it can be concluded that brick-shaped particles are the most suitable and platelet-shaped particles are the least suitable for heat exchanger performance enhancement. It may be noted that both viscosity and thermal conductivity of nanofluids enhance with an increase in nanoparticle surface area-to-volume ratio, and the change in heat exchanger performance index depends on a relative increase in viscosity and thermal conductivity.

It has been found from the investigation that area and pump work both reduce with the use of hybrid nanofluids. The annual cost depends on the maintenance cost and the operating cost, which in turn depends on the area of the plate and pump work required. Hence the annual cost of milk chilling unit can be decreased by using the hybrid nanofluids.

Conclusions

Performance enhancement of a refrigeration unit has been assessed using various brines and respective hybrid nanofluids as a secondary refrigerant with plate evaporator for milk chilling application. Results show that PG and EG brine-based CuO–Cu hybrid nanofluids are better as a secondary refrigerant due to enhanced heat transfer characteristics and the reduced heat transfer area that leads to a reduction in price and space required. Moreover, silica–copper hybrid nanofluid is better as a secondary refrigerant due to enhanced exergetic efficiency, pump work and performance index of the plate evaporator. Also, the particles with smaller size and brick shape are preferable as nanoparticles for improving the performance of the heat exchangers for the milk chilling application. Platelet-shaped particles show a decrement in the performance index because the viscosity of hybrid nanofluid with this shaped nanoparticle is more in comparison with other shape hybrid nanofluid. Therefore, the brine-based hybrid nanofluids having brick-shaped smaller-sized nanoparticles are being suggested as a better replacement for the secondary refrigerant as they can enhance the performance of plate evaporators at low temperatures with reduced consumption of primary coolant and hence reduce the chances of accidents due to their leakage.

References

1. Wang K, Eisele M, Hwang Y, Radermacher R. Review of secondary loop refrigeration systems. Int J Refrig. 2010;33:212–34.
2. Hillerns F. Thermophysical properties and corrosion behavior of secondary coolants. Atlanta: ASHRAE Winter Meeting; 2001. p. 1–6.
3. Bhattad A, Sarkar J, Ghosh P. Improving the performance of refrigeration systems by using nanofluids: a comprehensive review. Renew Sustain Energy Rev. 2018;82:3656–69.
4. Shadloo MS, Mahian O. Recent advances in heat and mass transfer. J Therm Anal Calorim. 2019;135:1611–5.
5. Mahian O, Bajestan EE, Poncet S. Nanofluid today. J Therm Anal Calorim. 2019;135:23–8.
6. Sarkar J, Ghosh P, Adil A. A review on hybrid nanofluids: recent research, development and applications. Renew Sustain Energy Rev. 2015;43:164–77.
7. Babar H, Ali HM. Towards hybrid nanofluids: preparation, thermophysical properties, applications, and challenges. J Mol Liq. 2019;281:598–633.
8. Yang L, Ji W, Zhang Z, Jin X. Thermal conductivity enhancement of water by adding graphene nanosheets: consideration of particle loading and temperature effects. Int Commun Heat Mass transf. 2019;109:104353.
9. Yang L, Mao M, Huang JN, Ji W. Enhancing the thermal conductivity of SAE 50 engine oil by adding zinc oxide nano-powder: an experimental study. Powder Technol. 2019;356:335–41.
10. Moldoveanu GM, Huminic G, Minea AA, Huminic A. Experimental study on thermal conductivity of stabilized Al_2O_3 and SiO_2 nanofluids and their hybrid. Int J Heat Mass Transf. 2018;127:450–7.
11. Rashidi S, Mahian O, Languri EM. Applications of nanofluids in condensing and evaporating systems: a review. J Therm Anal Calorim. 2018;131:2027–39.
12. Rashidi S, Karimi N, Mahian O, Esfahani JA. A concise review on the role of nanoparticles upon the productivity of solar desalination systems. J Therm Anal Calorim. 2019;135:1145–59.
13. Yang L, Huang JN, Ji W, Mao M. Investigations of a new combined application of nanofluids in heat recovery and air purification. Powder Technol. 2019. https://doi.org/10.1016/j.powtec.2019.10.053.
14. Kumar V, Sarkar J. Numerical and experimental investigations on heat transfer and pressure drop characteristics of Al_2O_3–TiO_2 hybrid nanofluid in minichannel heat sink with different mixture ratio. Powder Technol. 2019;345:717–27.
15. Bhattad A, Sarkar J, Ghosh P. Experimentation on effect of particle ratio on hydrothermal performance of plate heat exchanger using hybrid nanofluid. Appl Therm Eng. 2019;162:114309.
16. Singh SK, Sarkar J. Energy, exergy and economic assessments of shell and tube condenser using hybrid nanofluid as coolant. Int Commun Heat Mass Transf. 2018;98:41–8.
17. Tiwari AK, Ghosh P, Sarkar J. Particle concentration levels of various nanofluids in plate heat exchanger for best performance. Int J Heat Mass Transf. 2015;89:1110–8.
18. Huang D, Wu Z, Sunden B. Effects of hybrid nanofluid mixture in plate heat exchangers. Exp Therm Fluid Sci. 2016;72:190–6.
19. Kumar V, Tiwari AK, Ghosh SK. Effect of variable spacing on performance of plate heat exchanger using nanofluids. Energy. 2016;114:1107–19.
20. Bhattad A, Sarkar J, Ghosh P. Exergetic analysis of plate evaporator using hybrid nanofluids as secondary refrigerant for low-temperature applications. Int J Exergy. 2017;24–1:1–20.
21. Kumar V, Tiwari AK, Ghosh SK. Exergy analysis of hybrid nanofluids with optimum concentration in a plate heat exchanger. Mater Res Express. 2018;5:065022.
22. Bhattad A, Sarkar J, Ghosh P. Energy-economic analysis of plate evaporator using brine-based hybrid nanofluids as secondary refrigerant. Int J Air-Cond Refrig. 2018;26(1):1850003-12.
23. Bhattad A, Sarkar J, Ghosh P. Energetic and exergetic performances of plate heat exchanger using brine based hybrid nanofluid for milk chilling application. Heat Transf. Eng. 2019; 1–14. https://doi.org/10.1080/01457632.2018.1546770.
24. Li CH, Peterson GP. The effect of particle size on the effective thermal conductivity of Al_2O_3–water nanofluids. J Appl Phys. 2007;101:044312.
25. Timofeeva EV, Routbort JL, Singh D. Particle shape effects on thermophysical properties of alumina nanofluids. J Appl Phys. 2009;106:014304.
26. Jeong J, Li C, Kwon Y, Lee J, Kim SH, Yun R. Particle shape effect on the viscosity and thermal conductivity of ZnO nanofluids. Int J Refrig. 2013;36:2233–41.
27. Nazarabada MK, Goharshadi EK, Youssefi A. Particle shape effects on some of the transport properties of tungsten oxide nanofluids. J Mol Liq. 2016;223:828–35.
28. Nemati Z, Alonso J, Rodrigo I, Das R, Garaio E, García JÁ, Orue I, Phan M-H, Srikanth H. Improving the heating efficiency of iron oxide nanoparticles by tuning their shape and size. J Phys Chem C. 2018;122:2367–81.
29. Shaiq S, Maraj EN, Iqbal Z. A comparative analysis of shape factor and thermophysical properties of electrically conducting nanofluids TiO_2–EG and Cu–EG towards stretching cylinder. Chaos Soliton Fract. 2019;118:290–9.
30. Yang L, Zhang Z, Du K. Heat transfer and flow optimization of a novel sinusoidal minitube filled with non-Newtonian

SiC/EG–water nanofluids. Int J Mech Sci. 2019. https://doi.org/10.1016/j.ijmecsci.2019.105310.
31. Yang L, Ji W, Huang JN, Xu G. An updated review on the influential parameters on thermal conductivity of nanofluids. J Mol Liq. 2019. https://doi.org/10.1016/j.molliq.2019.111780.
32. Elias MM, Miqdad M, Mahbubul IM, Saidur R, Kamalisarvestani M, Sohel MR, Hepbasli A, Rahim NA, Amalina MA. Effect of nanoparticle shape on the heat transfer and thermodynamic performance of a shell and tube heat exchanger. Int Commun Heat Mass Transf. 2013;44:93–9.
33. Mahian O, Kianifar A, Heris SZ, Wongwises S. First and second laws analysis of a minichannel-based solar collector using boehmite alumina nanofluids: effects of nanoparticle shape and tube materials. Int J Heat Mass Transf. 2014;78:1166–76.
34. Arani AAA, Sadripour S, Kermani S. Nanoparticle shape effects on thermal-hydraulic performance of boehmite alumina nanofluids in a sinusoidal–wavy mini-channel with phase shift and variable wavelength. Int J Mech Sci. 2017;128–129:550–63.
35. Hajabdollahi H, Hajabdollahi Z. Numerical study on impact behavior of nanoparticle shapes on the performance improvement of shell and tube heat exchanger. Chem Eng Res Des. 2017;125:449–60.
36. Xie H, Wang J, Xi T, Liu Y, Ai F, Wu Q. Thermal conductivity enhancement of suspensions containing nanosized alumina particles. J Appl Phys. 2002;91:4568–72.
37. Kim SH, Choi SR, Kim D. Thermal conductivity of metal-oxide nanofluids: particle size dependence and effect of laser irradiation. J Heat Transf. 2006;129:298–307.
38. Nguyen CT, Desgranges F, Roy G, Galanis N, Maré T, Boucher S, Mintsa HA. Temperature and particle-size dependent viscosity data for water-based nanofluids–hysteresis phenomenon. Int J Heat Fluid Flow. 2007;28:1492–506.
39. Mintsa HA, Roy G, Nguyen CT, Doucet D. New temperature dependent thermal conductivity data for water-based nanofluids. Int J Therm Sci. 2009;48:363–71.
40. Monfared M, Shahsavar A, Bahrebar MR. Second law analysis of turbulent convection flow of boehmite alumina nanofluid inside a double-pipe heat exchanger considering various shapes for nanoparticle. J Therm Anal Calorim. 2019;135:1521–32.
41. Klein SA. Engineering Equation Solver Professional. Version V10.042-3D, USA: F-Chart, 2016.
42. Zarringhalam M, Karimipour A, Toghraie D. Experimental study of the effect of solid volume fraction and Reynolds number on heat transfer coefficient and pressure drop of CuO–water nanofluid. Exp Therm Fluid Sci. 2016;76:342–51.
43. Huang D, Wu Z, Sunden B. Pressure drop and convective heat transfer of Al_2O_3/water and MWCNT/water nanofluids in a chevron plate heat exchanger. Int J Heat Mass Transf. 2015;89:620–6.
44. Kakac S, Liu H. Heat exchangers: selection, rating and thermal design. 2nd ed. Boca Raton: CRC Press LLC; 2002.
45. Chougule SS, Sahu SK. Model of heat conduction in hybrid nanofluid. ICECCN: IEEE: 2013.
46. Corcione M. Heat transfer features of buoyancy-driven nanofluids inside rectangular enclosures differentially heated at the sidewalls. Int J Therm Sci. 2010;49–9:1536–46.
47. Sahu M, Sarkar J. Steady-state energetic and exergetic performances of single-phase natural circulation loop with hybrid nanofluids. J Heat Transf. 2019;141:082401.
48. Sheikholeslami M, Shamlooei M. Magnetic source influence on nanofluid flow in porous medium considering shape factor effect. Phys Lett A. 2017;381:3071–8.
49. Elias MM, Shahrul IM, Mahbubul IM, Saidur R, Rahim NA. Effect of different nanoparticle shapes on shell and tube heat exchanger using different baffle angles and operated with nanofluid. Int J Heat Mass Transf. 2014;70:289–97.